Composition-Tuned Co_nSi Nanowires: Location-Selective Simultaneous Growth along Temperature Gradient

Kwanyong Seo,[†] Sunghun Lee,[†] Hana Yoon,[†] Juneho In,[†] Kumar S. K. Varadwaj,[†] Younghun Jo,[‡] Myung-Hwa Jung,[§] Jinhee Kim,[∥] and Bongsoo Kim[†,*]

[†]Department of Chemistry, KAIST, Daejeon 305-701, Korea, [‡]Quantum Material Research Team, KBSI, Daejeon 305-333, Korea, [§]Department of Physics, Sogang University, Seoul 121-742, Korea, and [∥]Center for Nanoscience and Quantum Metrology, KRISS, Daejeon 305-600, Korea

ABSTRACT We report the simultaneous and selective synthesis of single-crystalline Co_nSi NWs ($n = 1-3$) and their corresponding crystal structures—simple cubic (CoSi), orthorhombic (Co_2Si), and face-centered cubic (Co_3Si)—following a composition change. Co_nSi NWs were synthesized by placing the sapphire substrates along a temperature gradient. The synthetic process is a successful demonstration of tuning the chemical composition in Co_nSi NWs. The synthesis and detailed crystal structure of single-crystalline Co_2Si and Co_3Si are reported for the first time including the bulk and the nanostructure phases. The electrical and magnetic properties of Co_2Si NWs are investigated and compared with those of CoSi NWs.

KEYWORDS: nanowires · transition metal silicides · cobalt silicide · single-crystalline · crystal engineering · metastable compounds

Transition metal silicides can form stable crystal structures over a wide range of composition, and often their constituent metal atoms can be partially substituted by other metal atoms while the same crystal structure is maintained.[1−3] Because of this, transition metal silicides exhibit a highly rich spectrum of physical properties. Fe_5Si_3, for example, is a high-temperature ferromagnetic material with Curie temperature (T_c) of 381 K, and Fe_3Si shows a half-metallic property with T_c of 840 K.[4−6] On the other hand, ternary silicides such as $Fe_{1-x}Co_xSi$ exhibit unusual positive magnetoresistance (MR) and a large anomalous Hall effect while displaying a helimagnetic ordering.[7−9] Such diversities in the structures and physical properties make nanowires (NWs) of transition metal silicides very attractive and useful materials in the fields of spintronics, thermoelectrics, nanoelectronics, and field emission displays.[10−14]

Most of metal silicide NWs reported so far were synthesized in the gas phase.[15−27] Because we have to maintain both the metal to silicon ratio and degree of supersaturation at appropriate values simultaneously, changing the composition of metal silicide NWs in a wide range has been rather difficult. Finding effective methods to synthesize metal silicide NWs in various compositions is, therefore, indispensible for development of practical nanodevices utilizing versatile physical properties of these NWs. We have not fully understood, however, the crystal structures and physical properties of most of the metastable phases of metal silicides even in a bulk form because of their structural instability at room temperature. Because thermodynamically metastable modifications can be stabilized in nanostructures,[28] novel metal silicide structures can be synthesized in the form of NWs. Hence, synthesizing composition-tuned metal silicide NWs would provide opportunities to explore various materials of novel and interesting properties and to investigate the correlation between the crystal structures and the physical properties.

Here we report the simultaneous and location-dependent selective synthesis of Co_nSi NWs ($n = 1-3$) and their corresponding crystal structures—simple cubic (CoSi), orthorhombic (Co_2Si), and face-centered cubic (fcc) (Co_3Si)—following a composition change.

RESULTS AND DISCUSSION

We demonstrated previously that on the Si substrate at a high temperature only CoSi NWs are formed by the following reaction.[25]

$$2CoCl_2(g) + 3Si(s) \leftrightarrow 2CoSi(s) + SiCl_4(g) \quad \text{[on a Si substrate]} \qquad (1)$$

No other phases of cobalt silicide were obtained on the Si substrate in the above reaction because only the thermodynamically

*Address correspondence to bongsoo@kaist.ac.kr.

Received for review February 25, 2009 and accepted April 18, 2009.

Published online April 23, 2009.
10.1021/nn900191g CCC: $40.75

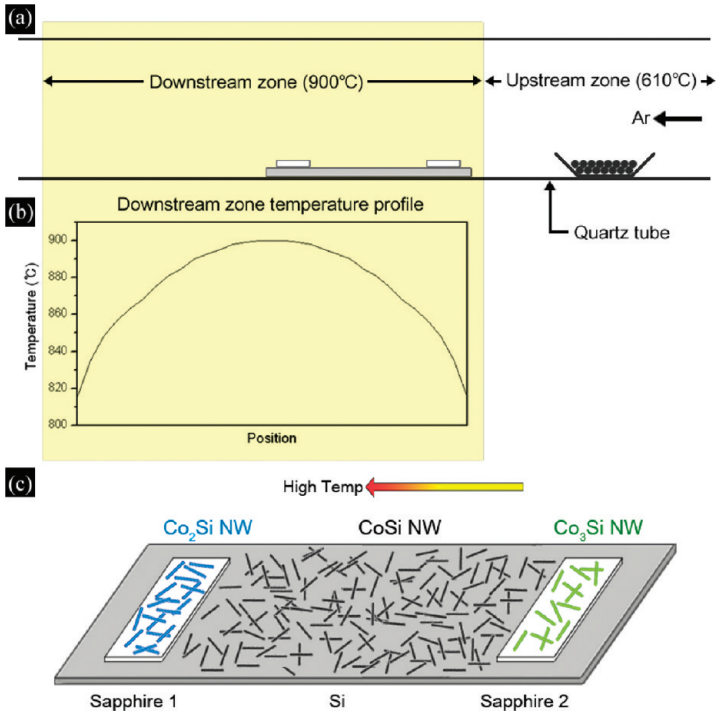

Figure 1. Experimental setup. (a) Horizontal tube furnace with two independently controlled heating zones. (b) Temperature profile indicates that the center of the downstream zone is at 900 °C, and the substrates are at 820−890 °C. (c) Tilted view illustration of the substrate placement in panel a. A rectangular Si wafer (50 mm × 15 mm) kept at the downstream zone played a role of Si source for NW synthesis. Co_2Si NWs are grown on the sapphire 1 substrate, CoSi NWs on the Si, and Co_3Si NWs on the sapphire 2.

most stable binary phase is produced in the solid-state reaction of Si substrate and $CoCl_2$. If we place a sapphire substrate on top of a Si wafer (Figure 1), however, NWs of a diverse cobalt−silicon ratio could be formed on the sapphire substrate since Si atoms are supplied from the $SiCl_4$ vapor instead of the Si substrate, and thus the reaction follows a different mechanism (reactions 2 and 3).[19]

$$6CoCl_2(g) + 3SiCl_4(g) \leftrightarrow 3Co_2Si + 12Cl_2(g) \quad \text{[on the sapphire 1]} \qquad (2)$$

$$6CoCl_2(g) + 2SiCl_4(g) \leftrightarrow 2Co_3Si + 10Cl_2(g) \quad \text{[on the sapphire 2]} \qquad (3)$$

In this case, the sapphire substrate does not participate in the reaction but only plays a role as a supporting plate on which the NWs grow through gas-phase reactions. Identical results were obtained when quartz plates were employed in place of the sapphire substrates.

The main idea of this work is to control the composition of the cobalt silicide NWs by adjusting the $SiCl_4$ concentration. When the $CoCl_2$ concentration is kept constant in reactions 2 and 3, the cobalt−silicon composition ratio is determined by the concentration of $SiCl_4$, which is produced in reaction 1. The production rate and thus the concentration of $SiCl_4$ is dependent on the reaction temperature. In our experimental setup, the temperature inside the furnace increases toward the center of the downstream zone (Figure 1b), thus the concentration of $SiCl_4$ can be varied by adjusting the position of the sapphire substrate. When the sapphire substrate is placed in the lower temperature region (sapphire 2 in Figure 1c), the Si wafer near the sapphire substrate is also at a lower temperature, leading to less supply of $SiCl_4$ gas by reaction 1. In this case, cobalt silicide NWs with higher cobalt−silicon ratio are synthesized (reaction 3). On the other hand, cobalt−silicon ratio of the NWs formed on the sapphire 1 substrate is lower than that on the sapphire 2 substrate because of its higher temperature. Hence, cobalt silicide NWs of different elemental compositions grow simultaneously on the sapphire substrates placed along a temperature gradient (Figure 1c).

Figure 2 shows morphologies and elemental compositions of the as-synthesized Co_nSi NWs examined by field emission scanning electron microscopy (SEM), transmission electron microscopy (TEM), and energy-dispersive X-ray spectrometry (EDS). The SEM images and low-resolution TEM images show NWs with lengths of tens of micrometers. No secondary growth or extra structural features were observed. Si concentration in the NWs grown on the different substrates ranges from about 50 to 15% by the TEM-EDS study (third column in Figure 2). These elemental compositions are consistent with the proposed reaction mechanisms. We note that the density of the NWs decreases when the Co−Si composition ratio in the NWs increases. This can be explained by the fact that the nucleation rate of NWs is proportional to the amount of Si source when the precursor ($CoCl_2$) concentration is fixed at a constant precursor temperature. NW growth process on a Si substrate is primarily based on three steps: interdiffusion of the reactant elements (Si and deposited Co) in the solid state, nucleation, and growth of the crystalline product. Only thermodynamically stable CoSi NWs can grow in the diffusion-limited solid-state reactions at a low degree of supersaturation.[16] In this case, the growth rate along the axial direction would be much faster than that on the sapphire substrate. This would suppress the radial growth, and only thin and long NWs can grow on the Si substrate. In contrast, the NWs with higher Co−Si compositions show larger diameters and more straight morphology, which can be explained by the gas-phase synthetic process of these NWs. The gas-phase-based reactions facilitate atomic level mixing of the precursors in the vapor phase on the sapphire substrate. The precursor vapors would contribute to both radial and axial growth, hence axial growth competes with radial growth.[29] More detailed investigations are required to explain these observed aspect ratio differences.

TEM analysis of these NWs indicates that three kinds of NWs, simple cubic CoSi, orthorhombic Co_2Si, and fcc

Co_3Si, have been synthesized. CoSi NWs are synthesized on the Si wafer, as reported previously, and have a single-crystalline B20 CoSi structure.[25] Only CoSi NWs, the thermodynamically stable phase, can grow on a Si wafer by the solid-phase reactions. Figure 3 shows the crystal structures of the NWs with Si composition of 33%. The selected area electron diffraction (SAED) study shows a regular spot pattern (Figure 3a), revealing the single-crystalline nature of the NWs. The spots can be fully indexed to the orthorhombic C37-type Co_2Si and demonstrate that the NW growth is along the [001] direction down the [$\bar{1}$30] zone axis. X-ray diffraction (XRD) data (*Pbnm*, JCPDS 04-0847)[30] and a high-resolution TEM image of a NW with clear lattice fringes (Figure 3b) confirm again that the NWs are composed of single-crystalline Co_2Si. The lattice spacings of the planes are measured to be 0.37 and 0.21 nm, agreeing well with the spacings of the (001) and (311) planes of an orthorhombic Co_2Si structure, respectively. The two-dimensional fast Fourier transform (FFT) of the lattice-resolved image obtained from the high-resolution TEM (inset in Figure 3b) can also be indexed to an orthorhombic structure.

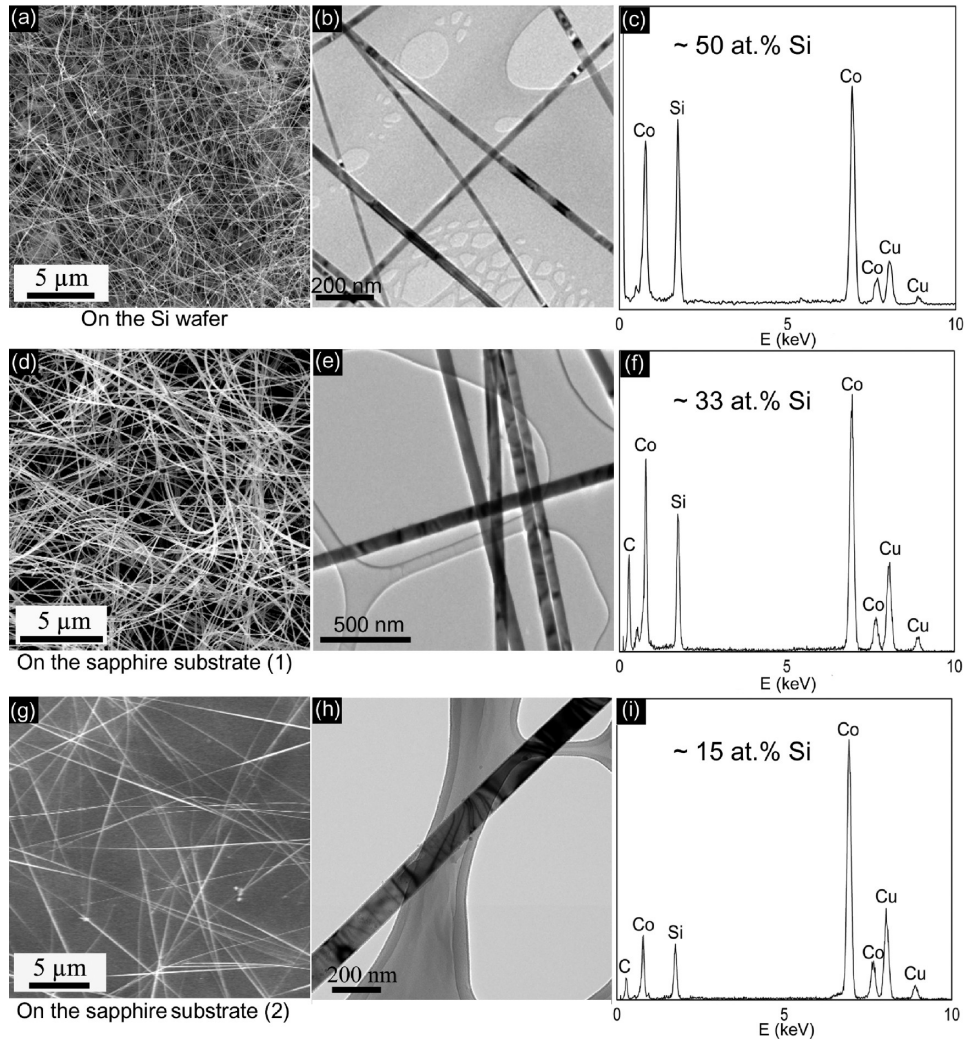

Figure 2. Change of the morphology and elemental concentrations of Si in the NWs grown at different growth environments. NWs grown on (a) Si wafer, (d) sapphire substrate 1, and (g) sapphire substrate 2 in Figure 1c. The low-resolution TEM images and TEM-EDS spectra corresponding to (a), (d), and (g) are shown in the second and third column.

Figure 4 shows the high-resolution TEM image and SAED patterns from various zone axes of the NWs with Si composition of 15%. In spite of numerous investigations on the crystallization and structure formation of Co−Si alloys, the Co-rich structures (especially over 70 at % Co case) have not been fully understood. During the cooling process in the bulk, metastable Co-rich structures are separated into many stable phases such as Co and Co_2Si. While we initially considered standard Co structures of hcp and fcc in order to analyze the TEM results, we find no similarity between the observed TEM results and the references. The simulation by Malozemoff *et al.*, however, indicated that the Co_3Si structure has almost the same lattice parameters as those of fcc Fe_3Si.[31] Therefore, we tried to identify the crystal structure of the Co-rich NWs indirectly with reference to the fcc Fe_3Si structure. We took SAED patterns from the various zone axes to make more accurate analysis of the crystal structure of the

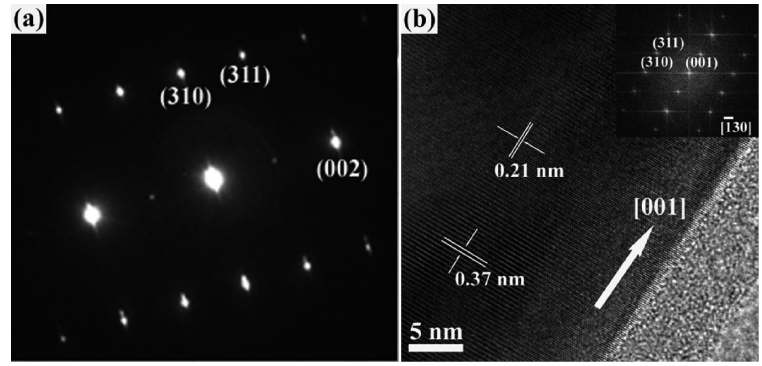

Figure 3. Detailed structural analysis of the NWs with Si concentration of 33 at %, shown in Figure 2d. (a) SAED pattern of the NW from the [$\bar{1}$30] zone axis. (b) High-resolution TEM image. The labeled distances of 0.37 and 0.21 nm correspond to the (001) and (311) planes, respectively, and the arrow shows [001] direction. Inset in (b) shows the FFT.

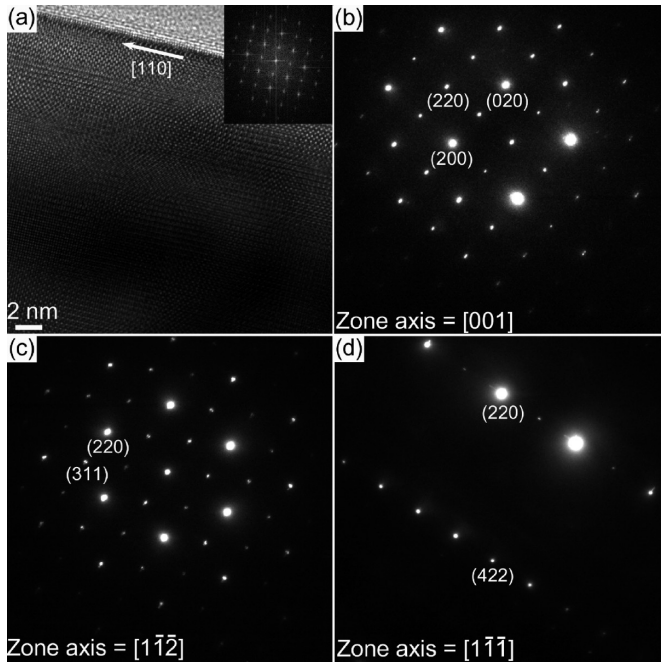

Figure 4. Detailed structural analysis of the NWs with Si concentration of 15 at %, shown in Figure 2g. (a) High-resolution TEM image. The arrow shows the [110] direction. Inset in (a) shows the FFT. SAED patterns of Co_3Si NW from the various zone axes: (b) [001], (c) [1$\bar{1}\bar{2}$], and (d) [1$\bar{1}\bar{1}$].

NWs (Figure 4b−d) and found that all these clear SAED patterns match well to the fcc Fe_3Si structure. According to this analysis, the NWs grow along the [110] direction. Interestingly, Si compositions of these Co-rich NWs are in a broad range from 10 to 20% as revealed by repeated TEM-EDS measurements, while the NWs keep the same crystal structure. This result is consistent with the fact that Si concentration in metastable Co_3Si ranges from 10 to 20% in the phase diagram.[32] On the other hand, Si compositions for the CoSi and Co_2Si NWs show generally 50 and 33%, respectively, with much less deviations. The synthesis of Co_3Si NW shows for the first time that single-crystalline Co_3Si fcc structure can exist at room temperature.

We measured the electrical and magnetic properties of the Co_2Si NWs to find out how the physical properties of NWs vary with the change of composition and crystal structure of the NWs. Figure 5a shows the temperature dependence of magnetization measured at 100 Oe for as-grown Co_2Si NW ensemble on a sapphire substrate. The high-temperature data are well fitted by the Curie−Weiss law, $M = C_p/(T - \theta_p)$, where C_p is the Curie constant and θ_p is the paramagnetic Curie temperature. We obtained the θ_p value of −366.7 K. We note that the inverse magnetization starts to deviate from linearity for $T < T_c = 115$ K, which is attributable to the ferromagnetic ordering. This ferromagnetic signature is verified from the magnetic hysteresis loop (Figure 5b). The magnetic moment of the Co_2Si NW ensemble was obtained by subtracting the diamagnetic contribution from the sapphire substrate. The magnetization measured below T_c exhibits a rapid and nonlinear increase at lower fields and a linear increase at higher fields. This indicates the ferromagnetic property of the Co_2Si NWs, although the magnetization curve does not show a typical shape of ferromagnetic materials. On the other hand, the magnetization curves measured above T_c show almost linear response to the magnetic field, which is a typical paramagnetic behavior.

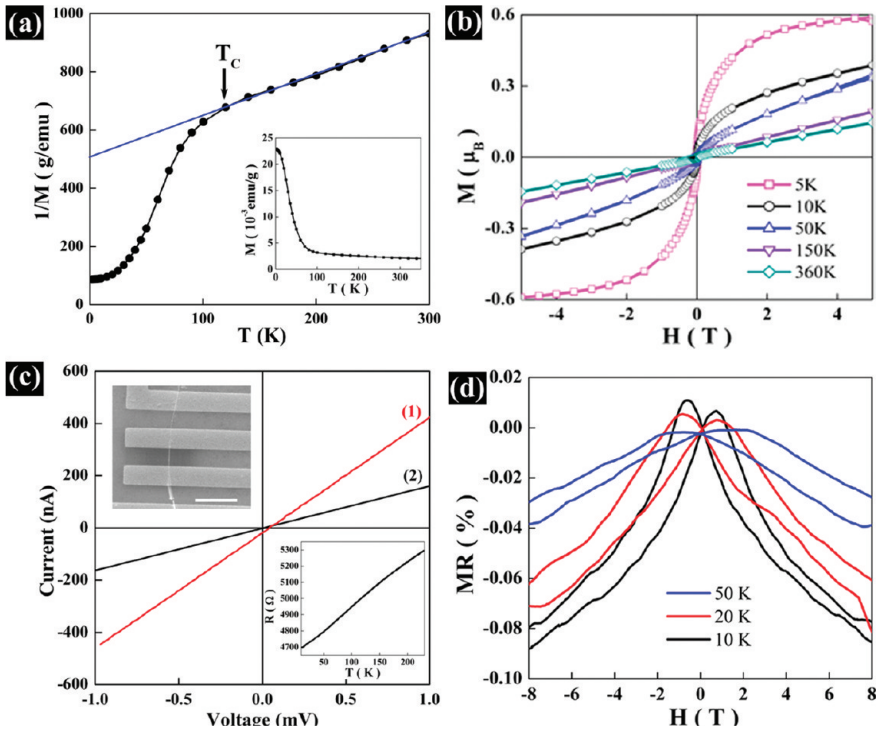

Figure 5. Electrical and magnetic properties of Co_2Si NWs. (a) Inverse magnetization *vs T* for the NW ensemble. Inset shows a plot of *M vs T* obtained from the NW ensemble at an applied field of 100 Oe. Arrow indicates the Curie temperature of 115 K. (b) Plot of *M* as a function of *H* obtained from the NW ensemble at 5 to 360 K. (c) *I vs V* curves recorded on a Co_2Si NW device (inset, upper left), with four- (line 1) and two- (line 2) probe measurements, respectively. *R vs T* curve shows typical metallic behavior (inset, lower right). (d) MR (%) curves of a single Co_2Si NW at various temperatures.

Figure 5c displays electrical transport data from the single NW device fabricated by standard e-beam lithography. The linear current *versus* voltage behavior at room temperature indicates an ohmic contact between the NW and electrodes. The resistivities of the two- and four-probe configurations are 546 and 200 $\mu\Omega \cdot$ cm, respectively, which match well with that reported for bulk single-crystal-

line Co_2Si (190 $\mu\Omega \cdot$ cm).[33] The higher value of two-probe resistivity is due to the contact resistance between the NW and electrodes. The resistance decreases monotonically with decreasing temperature from room temperature to 2 K. This is a typical metallic behavior. Figure 5d shows the standard longitudinal magnetoresistance (MR) data measured at various temperatures. The MR data are taken from a single Co_2Si NW device with four-probe. The MR measured below T_c shows a small peak structure around 2 T, which corresponds to the saturation field of magnetization. The MR ratio at 9 T is estimated to be 0.09% at 10 K and 0.04% at 50 K. The monotonic decrease of MR with increasing field is attributed to the reduction of magnetic scattering by magnetic ordering. No MR effect is observed above 50 K. The MR ratio is within our instrumental accuracy (~0.01%).

It has been very difficult to synthesize Co_2Si even in bulk due to its thermodynamic instability. While few reports are available referring to the physical properties of Co_2Si, conclusions are rather vague.[33−35] It is conjectured that the low T_c and weak ferromagnetic properties of Co_2Si measured in this work are attributable to the orthorhombic crystal structure.[36,37] Simple cubic CoSi is normally diamagnetic. For CoSi NWs with diameters less than 30 nm, the high percentage of surface Co atoms induces strong ferromagnetic properties of CoSi NWs,[25] which could not be confirmed in the case of Co_2Si NWs that are about 80 nm thick. Measurements of the physical properties of Co_3Si NWs are underway.

CONCLUSION

We have reported simultaneous synthesis of high-density freestanding single-crystalline Co_nSi NWs (n = 1−3) on different substrates. Composition-tuned selective growth of cobalt silicide NWs is achieved by placing sapphire substrates along a temperature gradient. TEM-EDS studies of the NWs indicated that Si concentration in the NWs grown on the series of substrates ranges from about 50 to 15%. Detailed crystal structures of the NWs are analyzed by high-resolution TEM, revealing that three kinds of NWs, simple cubic CoSi, orthorhombic Co_2Si, and fcc Co_3Si, have been synthesized. We have further reported that the crystal structure of the NWs affects the physical properties of the NWs indicated by the electrical and magnetic properties measurements on the Co_2Si NWs. These results indicate the possibility that metal silicide NWs of diverse electrical and magnetic properties can be synthesized by tuning the composition.

METHODS

Growth of Co_nSi Nanowires. Single-crystalline CoSi, Co_2Si, and Co_3Si NWs were synthesized in a horizontal hot-wall two-zone furnace with a 1 in. diameter inner quartz tube, as shown in Figure 1a. The setup is equipped with pressure and mass flow controllers. The upstream (US) zone and downstream (DS) zone were used for vaporization of precursor and NW growth, respectively. A rectangular Si wafer (50 mm × 15 mm) kept at the DS zone was the source of Si. The Co_2Si and Co_3Si NWs were grown on c-plane sapphire substrates placed on the Si wafer. This scheme provides convenient control of the Si composition in the NW. Anhydrous $CoCl_2$ powder (99.999%, Sigma-Aldrich) in an alumina boat was placed at the center of the US zone. The carrier argon gas was supplied through a mass-flow controller at the rate of 150−200 sccm. The substrates were placed at ~10 cm from the precursor position in the DS zone. Temperatures of the US zone and DS zone were maintained at 610 and 900 °C, respectively, for 20 min of reaction time, while the pressure was maintained at 500 Torr during the reaction. No catalyst was used for the NW synthesis.

Characterization. X-ray diffraction (XRD) patterns of the specimen were recorded on a Rigaku D/max-rc (12 kW) diffractometer operated at 40 kV and 80 mA with filtered 0.15405 nm Cu Kα radiation. Field emission scanning electron microscope (FESEM) images of Co_nSi NWs were taken on a Phillips XL30S. Transmission electron microscope (TEM) and high-resolution TEM (HRTEM) images and selected area electron diffraction (SAED) patterns were taken on a JEOL JEM-2100F transmission electron microscope operated at 200 kV. After nanostructures were dispersed in ethanol, a drop of the solution was put on the holey carbon coated copper grid for the preparation of TEM analysis.

Acknowledgment. This research was supported by KOSEF through NRL (ROA-2007-000-20127-0), SRC (R11-2005-008-00000-0), and CNMT (08K1501-02210) from MEST, Korea. M.-H.J. is supported by the Sogang University Research Grant (200810017.01).

Supporting Information Available: XRD spectrum of the Co_2Si NWs on c-plane sapphire substrate. This material is available free of charge *via* the Internet at http://pubs.acs.org.

REFERENCES AND NOTES

1. Manyala, N.; Sidis, Y.; DiTusa, J. F.; Aeppli, G.; Young, D. P.; Fisk, Z. Large Anomalous Hall Effect in a Silicon-Based Magnetic Semiconductor. *Nat. Mater.* **2004**, *3*, 255–262.
2. Manyala, N.; Sidis, Y.; DiTusa, J. F.; Aeppli, G.; Young, D. P.; Fisk, Z. Magnetoresistance from Quantum Interference Effects in Ferromagnets. *Nature* **2000**, *404*, 581–584.
3. Felser, C.; Fecher, G. H.; Balke, B. Spintronics: A Challenge for Materials Science and Solid-State Chemistry. *Angew. Chem., Int. Ed.* **2007**, *46*, 668–699.
4. Srivastava, P. C.; Tripathi, J. K. Giant Magnetoresistance (GMR) in Swift Heavy Ion Irradiated Fe Films on c-Silicon (Fe/c-Si). *J. Phys. D: Appl. Phys.* **2006**, *39*, 1465–1471.
5. Hines, W. A.; Menotti, A. H.; Budnick, J. I.; Burch, T. J.; Litrenta, T.; Niculescu, V.; Raj, K. Magnetization Studies of Binary and Ternary Alloys Based on Fe_3Si. *Phys. Rev. B* **1976**, *13*, 4060–4068.
6. Herfort, J.; Schönherr, H.-P.; Jenichen, B. Magnetic and Structural Properties of Ultrathin Epitaxial Fe_3Si Films on GaAs(001). *J. Appl. Phys.* **2008**, *103*, 07B506-1–07B506-3.
7. Uchida, M.; Onose, Y.; Matsui, Y.; Tokura, Y. Real-Space Observation of Helical Spin Order. *Science* **2006**, *311*, 359–361.
8. In, J.; Varadwaj, K. S. K.; Seo, K.; Lee, S.; Jo, Y.; Jung, M. H.; Kim, J.; Kim, B. Single Crystalline Ferromagnetic $Fe_{1-x}Co_xSi$ Nanowires. *J. Phys. Chem. C* **2008**, *112*, 4748–4752.
9. Schmitt, A. L.; Higgins, J. M.; Jin, S. Chemical Synthesis and Magnetotransport of Magnetic Semiconducting $Fe_{1-x}Co_xSi$ Alloy Nanowires. *Nano Lett.* **2008**, *8*, 810–815.
10. Zhou, F.; Szczech, J.; Pettes, M. T.; Moore, A. L.; Jin, S.; Shi, L. Determination of Transport Properties in Chromium Disilicide Nanowires *via* Combined Thermoelectric and Structural Characterizations. *Nano Lett.* **2007**, *7*, 1649–1654.

11. Szczech, J.; Schmitt, A. L.; Bierman, M. J.; Jin, S. Single-Crystal Semiconducting Chromium Disilicide Nanowires Synthesized *via* Chemical Vapor Transport. *Chem. Mater.* **2007**, *19*, 3238–3243.
12. Seo, K.; Varadwaj, K. S. K.; Cha, D.; In, J.; Kim, J.; Park, J.; Kim, B. Synthesis and Electrical Properties of Single Crystalline $CrSi_2$ Nanowires. *J. Phys. Chem. C* **2007**, *111*, 9072–9076.
13. Lin, Y.-C.; Lu, K.-C.; Wu, W.-W.; Bai, J.; Chen, L. J.; Tu, K. N.; Huang, Y. Single Crystalline PtSi Nanowires, PtSi/Si/PtSi Nanowire Heterostructures, and Nanodevices. *Nano Lett.* **2008**, *8*, 913–918.
14. Lin, H.-K.; Tzeng, Y.-F.; Wang, C.-H.; Tai, N.-H.; Lin, I.-N.; Lee, C.-Y.; Chiu, H.-T. Ti_5Si_3 Nanowire and Its Field Emission Property. *Chem. Mater.* **2008**, *20*, 2429–2431.
15. Wu, Y.; Xiang, J.; Yang, C.; Lu, W.; Lieber, C. M. Single-Crystal Metallic Nanowires and Metal/Semiconductor Nanowire Heterostructures. *Nature* **2004**, *430*, 61–65.
16. Kim, C. J.; Kang, K.; Woo, Y. S.; Ryu, K.-G.; Moon, H.; Kim, J.-M.; Zang, D.-S.; Jo, M.-H. Spontaneous Chemical Vapor Growth of NiSi Nanowires and Their Metallic Properties. *Adv. Mater.* **2007**, *19*, 3637–3642.
17. Kang, K.; Kim, S.-K.; Kim, C.-J.; Jo, M.-H. The Role of NiO_x Overlayers on Spontaneous Growth of $NiSi_x$ Nanowires from Ni Seed Layers. *Nano Lett.* **2008**, *8*, 431–436.
18. Chueh, Y.-L.; Ko, M.-T.; Chou, L.-J.; Chen, L.-J.; Wu, C.-S.; Chen, C.-D. $TaSi_2$ Nanowires: A Potential Field Emitter and Interconnect. *Nano Lett.* **2006**, *6*, 1637–1644.
19. Varadwaj, K. S. K.; Seo, K.; Lee, S.; Jo, Y.; Jung, M. H.; Kim, J.; Kim, B. Phase-Controlled Growth of Metastable Fe_5Si_3 Nanowires by a Vapor Transport Method. *J. Am. Chem. Soc.* **2007**, *129*, 8594–8599.
20. Ouyang, L.; Thrall, E. S.; Deshmukh, M. M.; Park, H. Vapor-Phase Synthesis and Characterization of ε-FeSi Nanowires. *Adv. Mater.* **2006**, *18*, 1437–1440.
21. Schmitt, A. L.; Bierman, M. J.; Schmeisser, D.; Himpsel, F. J.; Jin, S. Synthesis and Properties of Single-Crystal FeSi Nanowires. *Nano Lett.* **2006**, *6*, 1617–1621.
22. Schmitt, A. L.; Jin, S. Selective Patterned Growth of Silicide Nanowires without the Use of Metal Catalysts. *Chem. Mater.* **2007**, *19*, 126–128.
23. Song, Y.; Schmitt, A. L.; Jin, S. Ultralong Single-Crystal Metallic Ni_2Si Nanowires with Low Resistivity. *Nano Lett.* **2007**, *7*, 965–969.
24. Song, Y.; Jin, S. Synthesis and Properties of Single-Crystal β_3-Ni_3Si Nanowires. *Appl. Phys. Lett.* **2007**, *90*, 173122-1–173122-3.
25. Seo, K.; Varadwaj, K. S. K.; Mohanty, P.; Lee, S.; Jo, Y.; Jung, M. H.; Kim, J.; Kim, B. Magnetic Properties of Single-Crystalline CoSi Nanowires. *Nano Lett.* **2007**, *7*, 1240–1245.
26. Schmitt, A. L.; Zhu, L.; Schmeiber, D.; Himpsel, F. J.; Jin, S. Metallic Single-Crystal CoSi Nanowires *via* Chemical Vapor Deposition of Single-Source Precursor. *J. Phys. Chem. B* **2006**, *110*, 18142–18146.
27. Higgins, J. M.; Schmitt, A. L.; Guzei, I. A.; Jin, S. Higher Manganese Silicide Nanowires of Nowotny Chimney Ladder Phase. *J. Am. Chem. Soc.* **2008**, *130*, 16086–16094.
28. Mandl, B.; Stangl, J.; Martensson, T.; Mikkelsen, A.; Eriksson, J.; Karlsson, L. S.; Bauer, G.; Samuelson, L.; Seifert, W. Au-Free Epitaxial Growth of InAs Nanowires. *Nano Lett.* **2006**, *6*, 1817–1821.
29. Joyce, H. J.; Gao, Q.; Tan, H. H.; Jagadish, C.; Kim, Y.; Zhang, X.; Guo, Y.; Zou, J. Twin-Free Uniform Epitaxial GaAs Nanowires Grown by a Two-Temperature Process. *Nano Lett.* **2007**, *7*, 921–926.
30. See Supporting Information.
31. Malozemoff, A. P.; Williams, A. R.; Moruzzi, V. L. "Band-Gap Theory" of Strong Ferromagnetism: Application to Concentrated Crystalline and Amorphous Fe- and Co-Metalloid Alloys. *Phys. Rev. B* **1984**, *29*, 1620–1632.
32. Okamoto, H. *Desk Handbook: Phase Diagrams for Binary Alloys*; ASM International: Materials Park, OH, 2000.
33. Frolov, A. A.; Krentsis, R. P.; Sidorenko, F. A.; Gel'd, P. V. Some Physical Properties of Co_2Si and Ni_2Si in the 10−350 K Temperature Range. *Russ. Phys. J.* **1972**, *15*, 418–420.
34. Dézsi, I.; Engelmann, H.; Gonser, U.; Langouche, G. Cobalt−Silicide Structures Studied by Mössbauer Spectroscopy. *Hyperfine Interact.* **1987**, *33*, 161–171.
35. Díaz, J.; Morales, R.; Valvidares, S. M.; Alameda, J. M. Phase Separation in Fe−Si and Co−Si Sputtered Ferromagnetic Alloys and the Origin of Their Magnetic Anisotropy. *Phys. Rev. B* **2005**, *72*, 144413-1–144413-15.
36. Geller, S.; Wolontis, V. M. The Crystal Structure of Co_2Si. *Acta Crystallogr.* **1955**, *8*, 83–87.
37. Zhou, G. F.; Bakker, H. Atomically Disordered Nanocrystalline Co_2Si by High-Energy Ball Milling. *J. Phys.: Condens. Matter.* **1994**, *6*, 4043–4052.